2D-Mapping of the Catalyst Structure Inside a Catalytic Microreactor at Work: Partial Oxidation of Methane over Rh/Al_2O_3

Jan-Dierk Grunwaldt,*,† Stefan Hannemann,† Christian G. Schroer,‡ and Alfons Baiker†

Department of Chemistry and Applied Biosciences, ETH Zurich, CH-8093 Zurich, Switzerland and HASYLAB at DESY, Notkestrasse 85, D-22607 Hamburg, Germany

Received: January 18, 2006; In Final Form: March 1, 2006

Tremendous changes of the structure of Rh particles occurred during partial methane oxidation to hydrogen and carbon monoxide over a 2.5 wt % Rh/Al_2O_3 catalyst upon ignition of the catalytic reaction. Furthermore, near the ignition temperature a variation in the Rh-valence state along the catalyst bed was observed. By combining hard X-ray absorption spectroscopy (X-ray absorption near edge structure, XANES) with a charged coupled device (CCD) camera and using a suitable spectroscopic cell with gas supply and on-line mass spectrometry, we demonstrate that 2D-mapping of the Rh-oxidation state in a catalyst bed can be achieved during the catalytic reaction. For this purpose, X-ray images were recorded with the CCD camera at each energy around the Rh K-edge with and without the spectroscopic cell. This resulted effectively in the transmitted and incident intensity at each energy and at each pixel of the spectroscopic cell. Reconstruction of the full Rh K-edge XANES spectra at each pixel revealed the local distribution of oxidized and metallic Rh-species in the catalyst bed. Along the catalyst bed, structural changes were found with a steep gradient within less than 100 μm. Furthermore, a characteristic cone toward the inlet of the spectroscopic cell was observed.

1. Introduction

Structure−activity relationships gained by studying the catalysts at work are considered the key to further development of heterogeneous catalysts.[1−9] For this purpose, the physicochemical characterization techniques are adapted in a way that they can be applied during conditioning or under realistic reaction conditions. In situ X-ray absorption spectroscopy (XAS) is a well-established tool, since it can monitor both X-ray amorphous and crystalline structures even in gas phase, liquid phase or at high pressure.[2−4,10−12] Despite the growing number of in situ studies for identifying active sites in catalysts, spatial variation of the active site structure within the catalytic reactor has hardly been investigated up to now. However, mapping of a fluid inside a reactor using magnetic resonance imaging[13−16] and detection of temperature gradients using IR thermography[17] have uncovered strong differences in distributions of the fluid and the temperature under reaction conditions. Moreover, strong structural variations along a catalyst bed can occur if the conversion is close to 100% and/or the gas composition strongly changes along the catalyst bed as, e.g., encountered in partial oxidation reactions.[18]

Hence, in situ structural information on a catalyst with spatially resolved spectroscopic techniques is of substantial importance, which is the focus of the present study. To our knowledge, spatially resolved spectroscopic studies on a microscale providing structural information on a catalyst combined with catalytic activity have not been reported yet. Here, we chose X-ray absorption spectroscopy since hard X-rays can penetrate a number of materials and X-ray absorption spectra can give structural information even on amorphous materials such as encountered in supported noble metal catalysts. Principally, two different approaches can be chosen for 2D-imaging. Third-generation synchrotron radiation sources in combination with lenses or KB-mirrors (Kirkpatrick−Baez geometry) can provide highly focused hard X-ray beams which allow absorption spectroscopic scanning of the sample, applied in environmental science, material science, biology, etc.[19−24] On the other hand 2D-area detectors give the possibility to record locally resolved the intensity behind the sample.[25] The latter method has been chosen in the present study, since the parallel data acquisition leads to shorter recording times, particularly important in case of in situ studies.

The technique and potential of this strategy are demonstrated during partial methane oxidation over Rh/Al_2O_3. Catalytic partial oxidation of methane over supported noble metal particles is regarded one of the most promising processes for hydrogen production and gas-to-liquid technologies, particularly in chemical plants of medium size.[26−29] Rhodium is unique for its high resistance against carbon formation (cf. refs 29−31) and was thus selected for the present study. Previous in situ diffuse reflectance infrared Fourier transform spectroscopy (DRIFTS) and extended X-ray absorption fine structure (EXAFS) studies have shown strong structural changes of the Rh particles under reaction conditions.[31,32] Moreover, it is speculated that in the first part of the reactor the catalytic oxidation of methane and in the second part methane reforming is prevalent (combustion and reforming reactions, CRR, mechanism). Alternatively, a direct partial oxidation of methane is postulated, known as the direct partial oxidation (DPO) mechanism.[29] This should have important implications on the catalyst structure along the catalyst bed. In fact, modeling studies predict a change of the gas composition along the catalyst bed,[33] IR thermography indicated large temperature gradients between catalyst surface and the gas phase,[31] and recent preliminary studies unraveled an axial variation of the catalyst structure.[12] However, no final agreement

* Corresponding author phone: +41-44-632 30 93; fax: +41-44-632 11 63; e-mail: grunwaldt@chem.ethz.ch.
† ETH Zurich.
‡ HASYLAB at DESY.

10.1021/jp060371n CCC: $33.50
Published on Web 04/07/2006

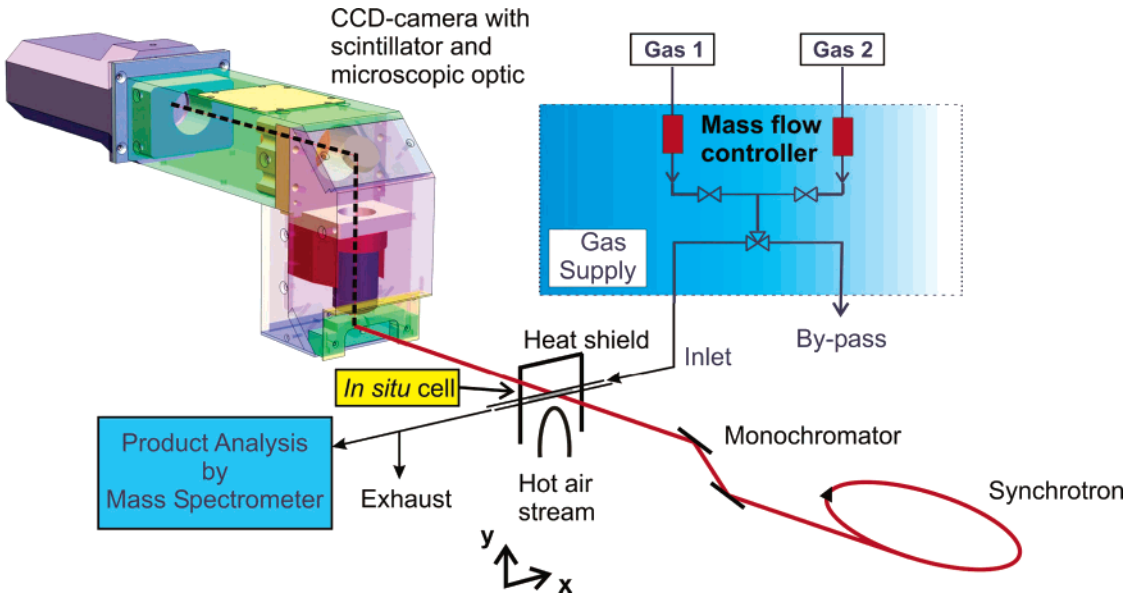

Figure 1. Strategy of the experiment for 2D-mapping of samples in the μm-scale. (1) The transmitted intensity is recorded by a CCD camera as function of the energy, and the position (x,y). (2) The X-ray energy is varied using white X-rays at a synchrotron and a double crystal Si(311) monochromator. (3) The catalytic experiment is performed in an X-ray transmittant capillary as in situ cell equipped with gas supply system and a mass spectrometer for determining the catalytic performance.

on the reaction mechanism has been achieved yet, mainly due to the difficulty in determining surface and bulk structures of the catalyst and their spatial variation in the reactor during operation. Hence, it is a well-suited example to demonstrate the feasibility of 2D-mapping of a catalyst under reaction conditions.

2. Experimental Section

Figure 1 gives an overview of the experimental strategy. The setup installed at the synchrotron consisted essentially of a glass capillary reactor, the gas supply system to provide the $6\%CH_4/3\%O_2$/He reaction mixture, and the analytical part (online mass spectrometer). The catalyst bed containing 2.5 wt $\%Rh/Al_2O_3$ (sieve fraction 100−200 μm) was fixed between two glass wool plugs in the in situ cell, heated by a hot air stream and mounted on an xy-table. Spatially resolved X-ray absorption was measured using a high-resolution X-ray camera by recording the X-ray intensity once without (incident intensity I_0) and with the spectroscopic cell (intensity I) as a function of energy E and position (x,y). In addition, "integral" spectra (averaged over the whole in situ cell) were taken using an ionization chamber before and behind the spectroscopic cell when dynamic changes of the gas flow conditions or the temperature were applied.

Sample Preparation. The Rh catalyst used in the present study was prepared by flame spray pyrolysis similar to a procedure described in ref 34. For this purpose, Rh(III)-acetylacetonate (ABCR) as precursor for the noble metal particles was dissolved in xylene together with 11 mL aluminum *sec*-butoxide (75% in butanol, Acros) as precursor for the support to a total volume of 40 mL.

The liquid mixtures were fed by a syringe pump (Inotech, 50 mL syringe, 3 mL·min^{-1}) via a capillary and dispersed with 3 L·min^{-1} O_2, forming a fine spray. This spray was surrounded and ignited by a small circular premixed methane−oxygen flame ring issuing from an annular gap (radius of 6 mm, 0.15 mm width). The total gas flow rate through the premixed methane/oxygen-supporting flame ring was 3.5 L·min^{-1} with a CH_4/O_2 ratio of 0.92. A stable combustion was achieved by applying a sheath gas (oxygen, 3.7 L/min, 99.8% Pan Gas) through a concentric sintered-metal ring. Calibrated mass flow controllers (Bronkhorst) were used to monitor all gas flows. The as-formed particles were collected on a glass-fiber filter (Whatman GF/D, 25.7 cm in diameter) placed on a cylinder mounted above the flame, by the aid of a vacuum pump (Vaccubrand). The surface area of the prepared Rh/Al_2O_3 catalyst was about 133 m^2/g. Electron microscopy evidenced a Rh-particle size of 2−3 nm.

Experimental Procedure for Integral X-ray Absorption Data. The experimental procedure for measuring X-ray absorption spectra in an integral manner was as follows: A sieved fraction (100−200 μm) of the $2.5\%Rh/Al_2O_3$ catalyst was fixed between two glass wool plugs in a 1.5 mm thick capillary (ca. 10 mm bed length) and tightened using Swagelok fittings, similar to that in refs 35 and 36. A flow of 15−20 mL/min was fed over the catalyst using mass flow controllers (Brooks) and the catalyst was heated to the respective reaction temperature using a rate of 5 °C/min. The temperature was measured by a thermocouple directly below the glass capillary. The maximum temperature that can be achieved with the setup is about 900 °C, using an appropriate airblower.[36] As reaction mixture methane and oxygen were used in a 2:1 ratio (premixed 6 vol % CH_4, 3 vol % O_2, in He). The whole in situ cell was mounted on an x,y-table, which allowed the capillary to align in both horizontal and vertical translation using step motors with an accuracy better than 1 μm.

X-ray absorption spectra were recorded at the Rh K-edge using a Si(311) double crystal monochromator. Higher harmonics were effectively removed by detuning of the crystals to 70% of the maximum intensity. The experiments were performed at beamline X1 at HASYLAB (DESY, Hamburg) typically with a beam size of 8 mm × 0.6 mm for integral measurements (averaging over most parts of the reactor) and 1 mm × 0.5 mm (horizontal × height) for mapping along the axial coordinate of the catalyst bed. The typical beam current of the storage ring was 80−120 mA (operating positron energy at 4.5 GeV). Ionization chambers (length 10 cm) served to detect the incoming X-ray intensity I_0 (100 mbar Kr) and the intensity of the transmitted X-rays using 400 mbar of Kr (in situ cell located

between the first and second ionization chamber, a Rh-reference foil for energy calibration between the second and third ionization chamber). Under stationary conditions before and after reaction and at 500 °C under reaction conditions EXAFS spectra were recorded around the Rh K-edge in the step scanning mode between 22 900 and 24 200 eV, respectively. Faster scans around the Rh K-edge (23 190 to 23 350 eV) were recorded using the normal step scanning EXAFS mode (ca. 4 min/scan) or the continuous EXAFS scanning mode (90 s/scan, QEXAFS).

The raw data were energy-calibrated (Rh K-edge energy of the Rh-foil: 23 220 eV, first inflection point), background corrected, and normalized using the WINXAS 3.0 software.[37] To quantify the relative ratio of oxidized Rh with respect to metallic Rh, linear combination analysis (LCA) of the XANES region around the edge was performed, using the spectra of the reduced and the oxidized (as prepared) materials for reconstruction. Instead, spectra of Rh-foil and Rh-oxide could be used as reference spectra for LCA-analysis. However, the XANES-region is usually strongly influenced by the cluster size (cf. ref 38) and, therefore, the oxidized and reduced catalyst were taken here.

Experimental Procedure for Spatially Resolved X-ray Absorption Data. With respect to the spectroscopic in situ cell, the same setup with heater, capillary, and on-line gas analysis by mass spectrometry was used. However, the X-ray absorption spectra were not taken by measuring the incoming intensity with the first ionization chamber and the outcoming intensity by a second ionization chamber. Instead a CCD (charged coupled device)-area detector was installed, as depicted in Figure 1. The incoming intensity $I_0(E, x, y)$ was measured by moving the capillary out of the beam and the transmitted intensity $I(E, x, y)$ by moving the capillary reactor into the beam with the y-translation. The X-ray energy was scanned in the XANES region around the Rh K-edge in steps of one eV (from $E =$ 23 190 to $E =$ 23 375 eV). The exposure time for each image was 30 s.

From these data, the absorption along the optical axis can be obtained for each pixel. To this end, the data is dark-field corrected, i.e., the influence of the CCD-dark current and read-out noise is removed by subtracting an averaged dark image (without X-rays) from each of the images. After this correction, each pixel value is proportional to the intensity $I(E, x, y)$ or $I_0(E, x, y)$ for images taken with or without sample, respectively. The integral absorption for each pixel and energy is obtained by

$$\int \mu(E,x,y,z) \cdot dz = -\ln \frac{I(E,x,y)}{I_0(E,x,y)}$$

For any given pixel in these images, a full absorption spectrum is available. These spectra can be compared to known reference spectra of different Rh species. Typically, the spectra characteristic for oxidized and reduced rhodium species were fitted together with the featureless component for uncharacteristic absorption to the measured data at each pixel, obtaining the relative quantity of oxidized and reduced Rh species over the whole catalyst bed. The distribution of both species inside the capillary, together with the distribution of other elements that show a featureless absorption spectrum in the given energy range could be obtained in this way.

3. Results

At first, spectra over the whole reactor bed were recorded at room temperature, then during heating to 400 °C. The integral

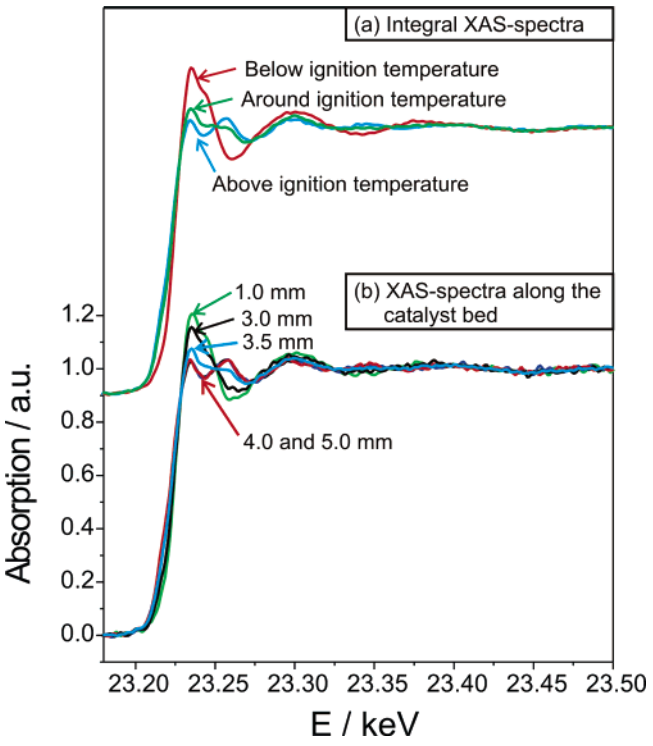

Figure 2. X-ray absorption spectra at the Rh K-edge of the 2.5 wt %Rh/Al_2O_3 catalyst (a) in an "integral" manner (averaged over the whole sample, beam 8 mm × 0.6 mm) below the ignition temperature (Rh-constituent oxidized reversibly), around the ignition temperature and above the ignition temperature (Rh-constituent reduced); (b) in a "local" manner probing at different positions of the catalyst bed with a 1 mm × 0.6 mm X-ray beam (at 283 °C).

spectra in Figure 2a unravel the rapid reduction of the Rh/Al_2O_3 catalyst during ignition of the partial oxidation reaction (e.g., the whiteline at 23 230 eV decreases and a new oscillation occurs at 23 260 eV). This is in line with previous results on Rh- and Ir-based catalysts.[32,39] Only for a short time a partly reduced Rh-catalyst was observed as intermediate in these integral spectra. In this case, the spectrum at the Rh K-edge can be fully reconstructed from the reduced and the oxidized Rh/Al_2O_3 catalyst. During cooling and heating cycles, the oxidation and reduction was observed to be reversible. This is schematically illustrated in Figure 3. The temperature of the capillary reactor and the oxidation state of the Rh-particles (extracted by linear combination analysis of the integral XANES) are depicted in the top graph of Figure 3, using the same color as in Figure 2a for the regions where oxidized, mixed (partly reduced) and reduced rhodium species were observed. Moreover, the traces in the on-line mass spectrometer analysis of several reactants and products/byproducts are given. It is obvious that the (partial) reduction of the Rh/Al_2O_3 catalyst is accompanied by the appearance of hydrogen in the feed. The total oxidation of methane to water and carbon dioxide occurred at lower temperatures with rhodium being in the oxidized state. No changes along the catalyst bed could be observed in this temperature region.

As Figure 3 (top) shows, after a certain time an intermediate oxidation state of the rhodium constituent (integral detection) could be stabilized at 283 °C ($t >$ 1.5 h). Closing down the slit size to 1 mm × 0.6 mm and scanning axially along the catalyst evidenced a strong change of the oxidation state of Rh (Figure 2b). Between 3 mm and 4 mm from the start of the catalytic bed, a tremendous change in structure occurred and, within the resolution of the beam, no gradient could be observed. Hence,

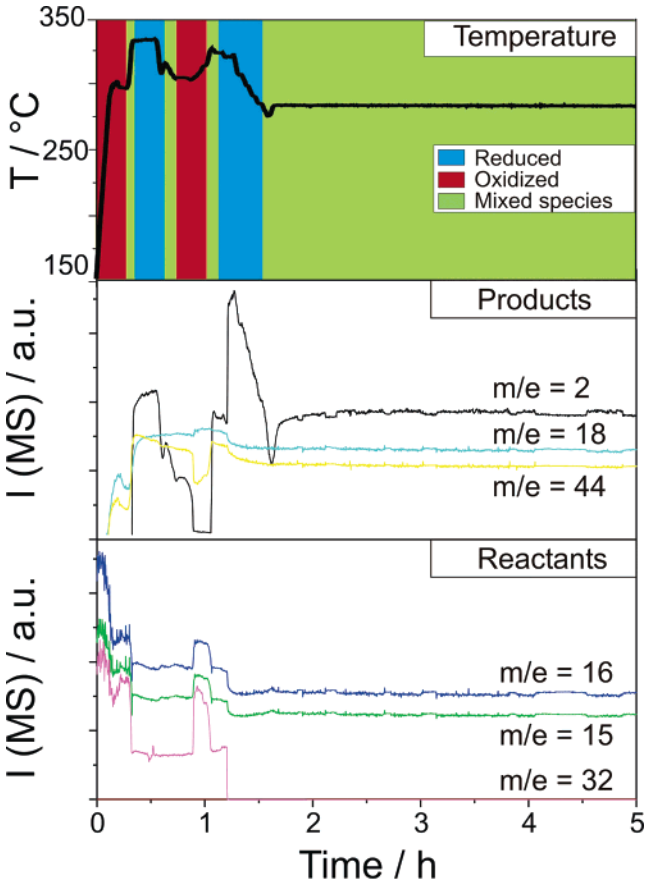

Figure 3. Temperature of the oven, product/byproducts ($m/e = 2$: hydrogen; $m/e = 18$: water; $m/e = 44$: carbon dioxide) and reactant concentration ($m/e = 15$: methane; $m/e = 32$: oxygen; $m/e = 16$: methane and oxygen) during the stabilization period of the experiment; the colors of the top graph indicate schematically whether the Rh-particles are oxidized (red), reduced (blue) or exhibit a mixed valence state (green); the 2D-mapping of the oxidation state inside the catalytic reactor was performed 2 h after start of the reaction while the catalytic activity was stable.

the gradient is much sharper than the probing beam and requires another approach, here achieved by 2D-mapping using a CCD-detector behind the microreactor (Figure 1). Note that the gradient was completely stable within the accuracy of the local probing. Also the catalytic conversion of methane including the product distribution was stable for more than 3 h (Figure 3). Hence, this state of the catalyst bed was ideally suited for 2D-mapping of the valence state of rhodium inside the spectroscopic plug flow reactor cell.

Figure 4 depicts the absorption for selected energies obtained from flat and dark-field corrected transmission images of the Rh/Al_2O_3 catalyst bed taken step by step at different energies during this time period. Obviously, at each energy, particles can be identified by their different (featureless) X-ray absorption. Below the energy of the Rh K-edge (<23 220 eV), the absorption is much smaller than above the edge (images at 23 230, 23 235, and 23 240 eV). Moreover, the absorption is similar over the whole catalyst bed below the Rh K-edge, whereas above the Rh K-edge, in particular at 23 235 and 23 240 eV, the absorption is higher on the left-hand side of the reactor (cf. Figure 4). Note that the gas was always fed from the left. The higher absorption (brighter spots on the left) can be explained with more oxidized Rh particles on the left side, since in this case, the absorption due to the pronounced whiteline absorption is much higher than for reduced Rh species (cf. absorption difference at 23 230 eV in Figure 2a).

This can be even more clearly observed in the movie, provided in the Supporting Information. In this movie, all the transmission images recorded step by step between 23 190 and 23 375 eV are shown. Running this movie shows the absorption as a function of energy (varied with time, energy given at the left top of each frame). The absorption (brighter pixels) increases above the Rh K-edge around 23 220 eV. Then, the stronger absorption on the inlet side of the spectroscopic cell (left) and even the modulation of the absorption above the edge can be observed (cf. the difference in the oxidized and reduced catalyst in Figure 2). Also note the high mechanical stability of the catalyst bed; only in the very end did some particles at the outlet of the reactor move, probably due to an instability in the exhaust system.

Hence, the absorption as function of position in the reactor (x,y) and energy E is fully represented by this movie (snapshot energy step by energy step). Reconstructing the X-ray absorption spectra for every position in the sectional area of the reactor and fitting them by least squares to spectra of the reduced Rh-species, oxidized Rh particles (mainly Rh^{3+}-species), and a linear background (featureless absorption by other elements), results in a 2D-map of the Rh-oxidation state distribution in the catalytic reactor, shown in Figure 5. On the left mainly oxidized Rh species are found (Figure 5a) while on the right the Rh-particles are reduced (Figure 5b). The featureless background (Figure 5c) takes track of the absorption of the support. In fact the spectra of every point (x,z) in the reactor could be fitted with low residual by these three contributions. The spectra for oxidized Rh and reduced Rh species at the left and at the right of the image are shown in Figure 5d, whose fingerprints well correspond to those in Figure 2. Obviously, there is a sharp gradient occurring within 100−200 μm inside the catalytic reactor that exhibits an elliptical shape (cone) of reduced rhodium species toward the inlet of the catalytic reactor. Moreover, more reduced species are rather allocated toward the top than toward the bottom of the reactor. This is further underlined by the distribution of Rh-species in Figure 6a, as calculated from Figure 5, and a selected profile shown in Figure 6b. The gradient was strikingly stable for several hours and it only changed its position after a change of the temperature or flow (not shown).

4. Discussion

Our study has demonstrated the potential of spatially resolved X-ray absorption spectroscopy during a heterogeneously catalyzed reaction. The study of the partial methane oxidation over Rh/Al_2O_3 shows that the structure changes tremendously within 100 μm. For this purpose, full field imaging with a 2D-detector with a resolution of 4 μm was chosen. This resulted in XANES data at every location inside the reactor which gave insight into the oxidation state of rhodium. Due to X-ray optical aspects and counting statistics, the resolution is limited to the 10 μm-range. Significant improvements of the spatial resolution are expected, when the experiment is carried out at third generation synchrotron radiation sources and by using area detectors with a higher resolution. Presently, a resolution of about 1 μm can be achieved in this way.[40−42] Alternatively, the use of highly focused X-ray beams (in scanning mode) may provide higher spatial resolution, but requires focusing optics and a fast monochromator.[22] X-ray microprobes are mostly used in combination with pre-scanning with microXRF to identify regions of interest.[20] However, this approach fails in the case of catalyst beds or in general for samples with similar concentration over the whole image. Then, probing with micro-

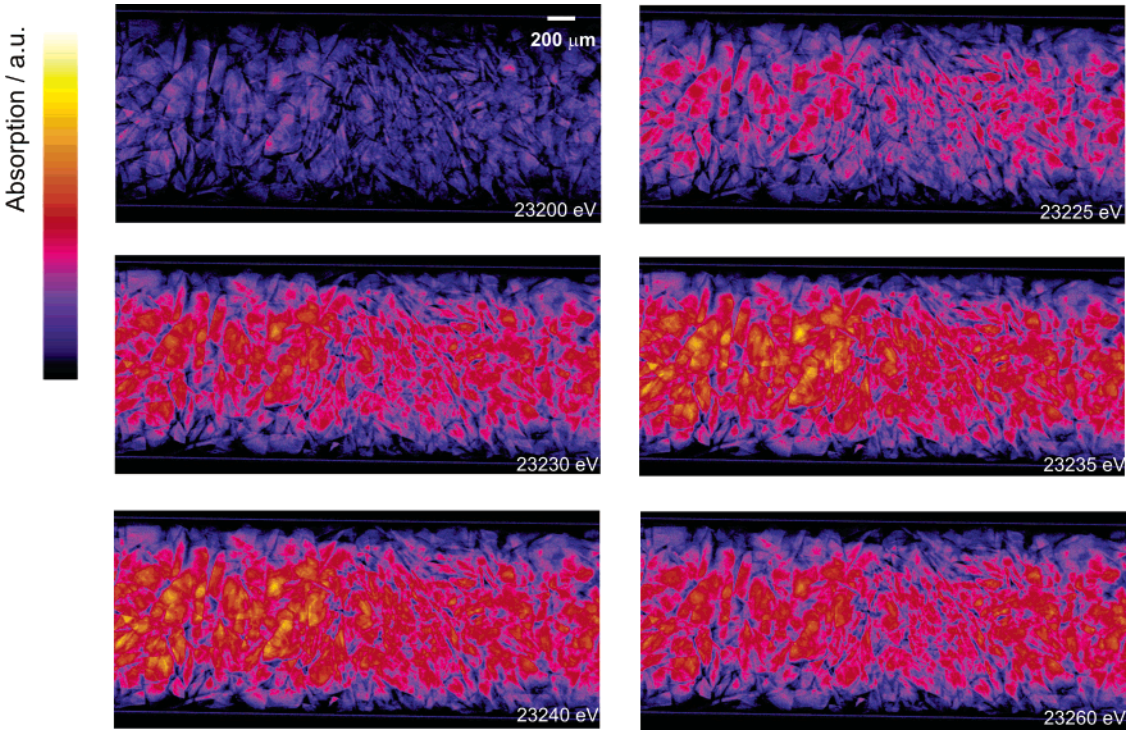

Figure 4. Flat- and dark-field corrected transmission images of Rh/Al_2O_3 inside the spectroscopic cell at different energies during the partial oxidation of methane at 283 °C (catalytic activity determined simultaneously, as depicted in Figure 2; during time period: $t = 2-6$ h); further snapshots are given in the ESI; the change of the absorption as function of energy is provided as movie in the electronic support information.

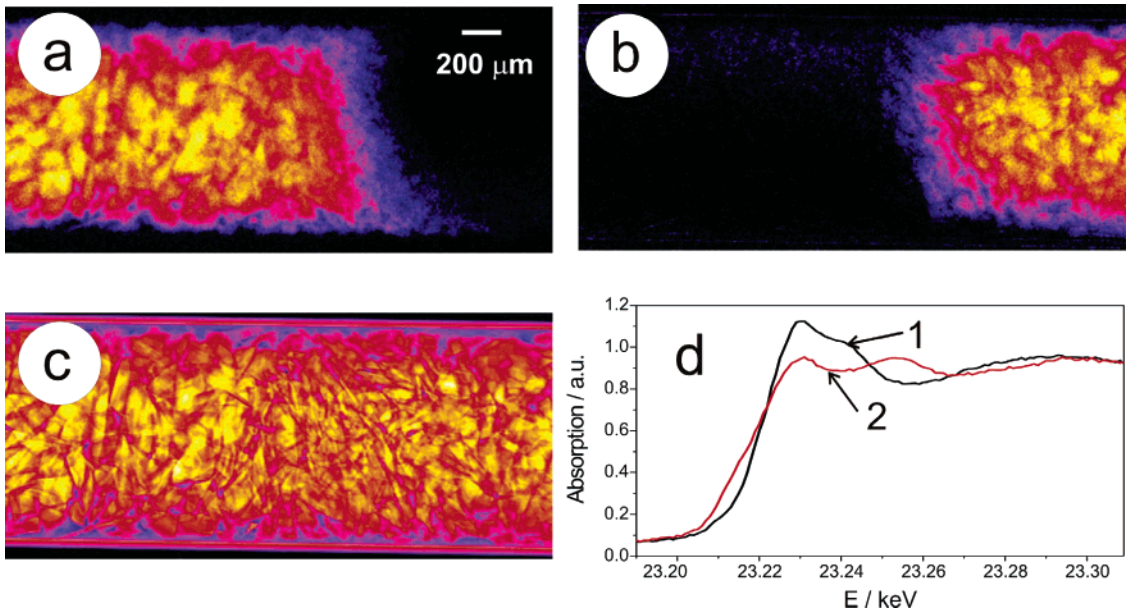

Figure 5. Amount of oxidized Rh-species (depicted in (a), oxidized species 1 in (d)), reduced Rh-species (depicted in (b), reduced species 2 in (d)) and the distribution of other elements that show a featureless absorption spectrum in the given energy range (c) along the capillary (original image taken by CCD-camera was 3.0 mm × 1.5 mm; the reaction gas mixture $6\%CH_4/3\%O_2$/He enters from the left).

probes suffers from long scanning times and requires fast scanning of the monochromator using, e.g., the quick-EXAFS mode.[22,43,44] In contrast, the strategy applied in the present study allowed us to determine a complete distribution of oxidized and reduced Rh species within a few hours due to simultaneous recording of all pixels. It can be expected that optimization of the scanning parameters (data points, acquiring data points with shorter time, and sources with higher intensity) will shorten this time even more, if necessary. Furthermore, profiles could be taken at characteristic points of the XAS-spectrum. This approach could also be used to "pre-scan" the sample, which is, in other fields, performed using micro-XRF, and then more detailed information at selected areas could be gained with X-ray microprobes. Most recent studies have demonstrated that hard X-rays can be focused down to 50 nm,[45,46] and the recent and present developments at synchrotron radiation sources with high brilliance will be beneficial for such studies offering higher resolution (cf. refs 47 and 48). In this respect, the higher resolution of soft X-rays as well as the X-ray absorption of adsorbed molecules is interesting (cf. refs 49, 50), but in this case, catalytic reactors or similar devices could not be penetrated due to the short penetration length of a few 10 micrometers.

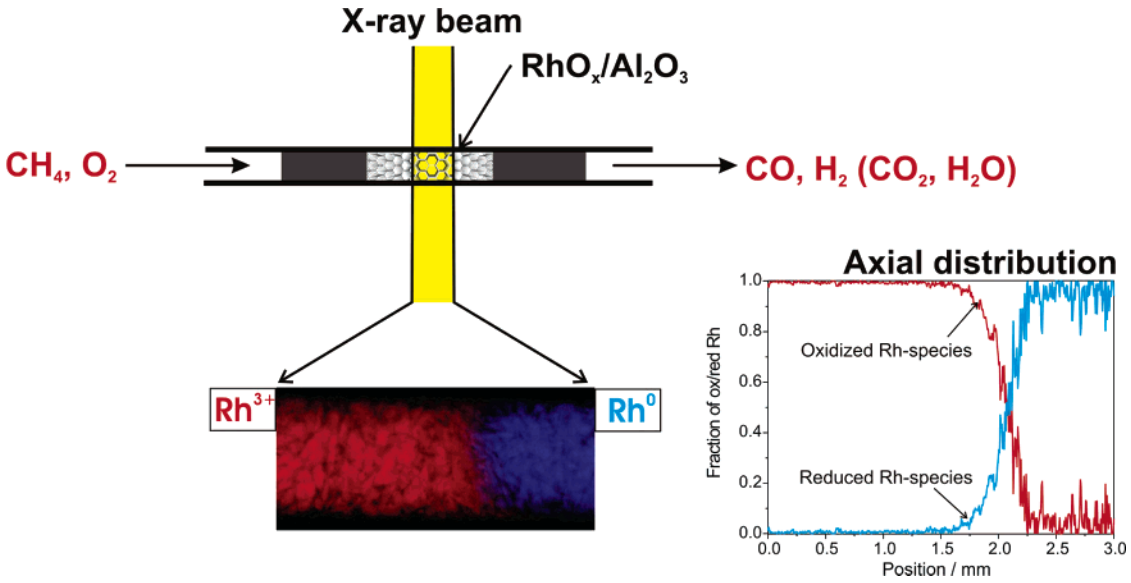

Figure 6. Distribution of oxidized Rh-species (i.e., Rh^{3+}, red) and reduced Rh-species (i.e., Rh^0, blue) in the spectroscopic cell (schematically shown) as derived from Figure 5(a) and 5(b); the axial distribution is taken from the middle of the fixed-bed reactor.

The study has given substantial insight into the ignition process of partial methane oxidation over supported Rh-particles. Interestingly, in the present system the Rh-particles are reoxidized during cooling that has not been observed on a 5% Rh/Al_2O_3 catalyst prepared via Rh-carbonyls.[32] However, at much lower noble metal loading, reoxidation of Rh-particles has been observed,[39] and in the present catalyst, the dispersion of Rh has been very high due to the special preparation process (flame spray pyrolysis, cf. experimental). Typically high dispersion and thus lower loadings are preferred to achieve a high accessibility of catalytically active noble metals.

A further interesting result is that the number of reduced particles is highest in the axis of the reactor and that the cone points toward the inlet. This indicates that the reaction occurs faster in the middle of the reactor. Probably due to the exothermic reaction and due to heat loss through the glass wall of the capillary; the temperature in the central region of the tubular reactor is higher than in its peripheral parts. Also modeling studies predict a change of the gas composition and temperature along the catalyst bed.[33] In addition, IR thermography indicated large temperature gradients between the catalyst surface and the gas phase.[31] The observed structural changes both in the axial and the radial direction of the catalyst bed support that both temperature and gas composition gradients occur in the fixed-bed reactor that significantly affect the catalyst structure. The observed profile further indicates that methane combustion at low temperature dominates in the first part of the reactor, whereas methane reforming occurs in the second part which corresponds to the CCR mechanism.[29] Due to the fact that the catalyst is fully oxidized when the formation of hydrogen and CO disappears indicates that metallic Rh species are crucial for the reaction mechanism and that hydrogen and CO are not directly formed from methane but rather by methane reforming. While total oxidation can occur over oxidized Rh particles, methane reforming is only observed as soon as metallic Rh particles are present. However, further studies at different temperatures are required to show, for example, that the reduction of Rh starts from the exit of the catalyst bed.

Partial methane oxidation is not the only reaction where strong changes of temperature and gas composition occur. Other reactions are, for example, CO-oxidation, partial oxidation of hydrocarbons, and steam reforming. Also in those cases, changes in the catalyst structure may occur and the technique applied here may be interesting as well. Furthermore, such in situ or *operando* spectroscopic information on the molecular structure of solids, as presented in our study, is not only interesting for monitoring a heterogeneous catalyst inside catalytic reactors. Recently, insights into the preparation of supported catalysts was gained by spatially resolved Raman and UV−visible−NIR spectroscopy.[51,52] Complementary information may be gained by EXAFS that has been successfully applied during the synthesis of solids,[12,53] and this has the advantage that high temperature and pressure can be applied.[2,4,12,36,54−56] It is also beneficial in areas such as electrocatalysis,[57−59] environmental sciences,[20,60−64] and sensor technology.[65,66] The elucidation of structure−property relationships is important for any type of functional materials and the possibility to detect spatial variations of the structure in situ, that is in general in the working state of the materials, will provide better control and deeper insight into their functioning.

5. Conclusions

Partial oxidation of methane over Rh-particles is a well-suited example to show the importance of spatially resolved 2D-monitoring of a catalyst inside a catalyst bed, since strong changes in the structure were observed upon ignition of the catalytic reaction along the catalyst bed. For the first time, we succeeded in developing a measuring strategy that allows in situ 2D-monitoring of a heterogeneous catalyst at work inside a spectroscopic cell using X-ray absorption spectroscopy. The structural changes were within a gradient of less than 100 μm. Possible applications of the strategy in various fields and its potential for 2D-imaging have been discussed.

Acknowledgment. We thank the Swiss Federal Institute of Technology and the Swiss Commission for Technology and Innovation (CTI, TopNano 21 grants 5978.2 TNS and 6740.1 TNS) for financial support. HASYLAB (beamline X1) is gratefully acknowledged for granting beamtime, and Mathias Herrmann (HASYLAB), Bernd Reime (HASYLAB) and Matteo Caravati (ETHZ) are thanked for their help during the measurements.

Supporting Information Available: Additional flat- and dark-field corrected transmission images of Rh/Al_2O_3 inside the

spectroscopic cell at different energies as well as a movie that shows the X-ray intensity behind the in situ cell as function of energy *E* (transformed into time scale). This material is available free of charge via the Internet at http://pubs.acs.org.

References and Notes

(1) Somorjai, G. A.; Thomas, J. M. Eds., *Top. Catal.* **1999**, *8*.
(2) Clausen, B. S. *Catal. Today* **1998**, *39*, 293.
(3) Thomas, J. M. *Angew. Chem., Int. Ed.* **1999**, *38*, 3589.
(4) Grunwaldt, J.-D.; Clausen, B. S. *Topics Catal.* **2002**, *18*, 37.
(5) Topsøe, H. *J. Catal.* **2003**, *216*, 155.
(6) Weckhuysen, B. M. *Chem. Commun.* **2002**, 97.
(7) Bazin, D.; Lynch, J.; Ramos-Fernandez, M. *Oil Gas Sci. Technol.* **2003**, *58*, 667.
(8) Brückner, A. *Catal. Rev. − Sci. Eng.* **2003**, *43*, 97.
(9) Banares, M. A. *Catal. Today* **2005**, *100*, 71.
(10) Iwasawa, Y. *X-ray absorption fine structure for catalysts and surfaces;* World Scientific: Singapore, 1996; Vol. 2.
(11) Newton, M. A.; Dent, A. J.; Evans, J. *Chem. Soc. Rev.* **2002**, *31*, 83.
(12) Grunwaldt, J. D.; Baiker, A. *Phys. Chem. Chem. Phys.* **2005**, *7*, 3526.
(13) Yuen, E. H. L.; Sederman, A. J.; Gladden, L. F. *Appl. Catal. A* **2002**, *232*, 29.
(14) Gladden, L. F. *Topics Catal.* **2003**, *24*, 19.
(15) Nott, K. P.; Heese, F. P.; Paterson-Beedle, M.; Macascie, L. E.; Hall, L. D. *Can. J. Chem. Eng.* **2005**, *83*, 68.
(16) Koptyug, I. V.; Lysova, A. A.; Sagdeev, R. Z.; Kirillov, V. A.; Kulikov, A. V.; Parmon, V. N. *Catal. Today* **2005**, *105*, 464.
(17) Li, B.; Maruyama, K.; Nurunnabi, M.; Kunimori, K.; Tomishige, K. *Ind. Eng. Chem. Res.* **2005**, *44*, 485.
(18) Grunwaldt, J.-D.; Baiker, A. *Catal. Lett.* **2005**, *99*, 5.
(19) Lengeler, B.; Schroer, C.; Tummler, J.; Benner, B.; Richwin, M.; A. Snigirev; Snigireva, I.; Drakopoulos, M. *J. Synchr. Radiat.* **1999**, *6*, 1153.
(20) Bertsch, P. M.; Hunter, D. B. *Chem. Rev.* **2001**, *101*, 1809.
(21) Proost, K.; Vincze, L.; Janssens, K.; Gao, N.; Bulska, E.; Schreiner, M.; Falkenberg, G. *X-ray Spectrom.* **2003**, *32*, 215.
(22) Schroer, C. G.; Kuhlmann, M.; Günzler, T. F.; Lengeler, B.; Richwin, M.; Griesebock, B.; Lützenkirchen-Hecht, D.; Frahm, R.; Ziegler, E.; Mashayekhi, A.; Haeffner, D. R.; Grunwaldt, J.-D.; Baiker, A. *Appl. Phys. Lett.* **2003**, *82*, 3360.
(23) Proost, K.; Janssens, K.; Wagner, B.; Bulska, E.; Schreiner, M. *Nucl. Instrum. Methods Phys. Res., Sect B* **2004**, *213*, 723.
(24) Vantelon, D.; Lanzirotti, A.; Scheinost, A. C.; Kretzschmar, R. *Environ. Sci. Technol.* **2005**, *39*, 4808.
(25) Rau, C.; Somogyi, A.; Simionovici, A. *Nucl. Instrum. Methods Phys. Res., Sect. B* **2003**, *203*, 444.
(26) Rostrupp-Nielsen, J. R. *Catal. Today* **1993**, *18*, 305.
(27) Ashcroft, A. T.; Cheetham, A. K.; Green, M. L. H.; Vernon, P. D. F. *Nature* **1991**, *352*.
(28) Hickman, D. A.; Schmidt, L. D. *Science* **1993**, *259*, 343.
(29) York, A. P. E.; Xiao, T. C.; Green, M. L. H. *Topics Catal.* **2003**, *22*, 345.
(30) Claridge, J. B.; Green, M. L. H.; Tsang, S. C.; York, A. P. E.; Ashcroft, A. T.; Battle, P. D. *Catal. Lett.* **1993**, *22*, 299.
(31) Basini, L.; Guarinoni, A.; Aragno, A. *J. Catal.* **2000**, *190*, 284.
(32) Grunwaldt, J.-D.; Basini, L.; Clausen, B. S. *J. Catal.* **2001**, *200*, 321.
(33) Schwiedernoch, R.; Tischer, S.; Correa, C.; Deutschmann, O. *Chem. Eng. Sci.* **2003**, *58*, 633.
(34) Stark, W. J.; Pratsinis, S. E.; Baiker, A. *Chimia* **2002**, *56*, 485.
(35) Clausen, B. S.; Steffensen, G.; Fabius, B.; Villadsen, J.; Feidenhans'l, R.; Topsøe, H. *J. Catal.* **1991**, *132*, 524.
(36) Grunwaldt, J.-D.; Caravati, M.; Hannemann, S.; Baiker, A. *Phys. Chem. Chem. Phys.* **2004**, *6*, 3037.
(37) Ressler, T. *J. Synchrotron. Radiat.* **1998**, *5*, 118.
(38) Bazin, D.; Rehr, J. J. *J. Phys. Chem. B* **2003**, *107*, 12398.
(39) Grunwaldt, J.-D.; Kappen, P.; Basini, L.; Clausen, B. S. *Catal. Lett.* **2002**, *78*, 13.
(40) Koch, A.; Raven, C.; Spanne, P.; Snigirev, A. *J. Opt. Soc. Am. A* **1998**, *15*, 1940.
(41) Globus, M.; Grinyov, B.; Ratner, M.; Tarasov, V.; Lyubinskiy, V.; Vydai, Y.; Ananenko, A.; Zorenko, Y.; Gorbenko, V.; Konstankevych, I. *IEEE Trans. Nucl. Sci.* **2004**, *51*, 1297.
(42) Di Michiel, M.; Merino, J. M.; Fernandez-Carreiras, D.; Buslaps, T.; Honkimaki, V.; Falus, P.; Martins, T.; Svensson, O. *Rev. Sci. Instrum.* **2005**, *76*.
(43) Frahm, R. *Physica B* **1989**, *158*, 342.
(44) Grunwaldt, J.-D.; Lützenkirchen-Hecht, D.; Richwin, M.; Grundmann, S.; Clausen, B. S.; Frahm, R. *J. Phys. Chem. B* **2001**, *105*, 5161.
(45) Mimura, H.; Matsuyama, S.; Yumoto, H.; Hara, H.; Yamamura, K.; Sano, Y.; Shibahara, M.; Endo, K.; Mori, Y.; Nishino, Y.; Tamasaku, K.; Yabashi, M.; Ishikawa, T.; Yamauchi, K. *Jpn. J. Appl. Phys.* **2005**, *44*, L539.
(46) Schroer, C. G.; Kurapova, O.; Patommel, J.; Boye, P.; Feldkamp, J.; Lengeler, B.; Burghammer, M.; Riekel, C.; Vincze, L.; van der Hart, A.; Küchler, M. *Appl. Phys. Lett.* **2005**, *87*, 124103.
(47) Grolimund, D.; Scheidegger, A. M.; Meyer, B.; Veen, J. F. v. d.; Abela, R. Layout of the microXAS Beamline at the SLS. In *PSI Scientific Report;* Paul Scherrer Institute: Villigen PSI, Switzerland, 2003; Vol III.
(48) Denecke, M.; Frahm, R.; Fröba, M.; Grunwaldt, J.-D.; Lützenkirchen-Hecht, D.; Röhler, J.; Welter, E. In *PETRA III Technical Design Report*; Balewski, K., Brefeld, W., Decking, W., Franz, H., Röhlsberger, R., Weckert, E., Eds.; Deutsches Elektronen-Synchrotron: Hamburg, Germany, 2004; p 334.
(49) Drake, I. J.; Liu, T. C. N.; Gilles, M.; Tyliszczak, T.; Kilcoyne, A. L. D.; Shuh, D. K.; Mathies, R. A.; Bell, A. T. *Rev. Sci. Instrum.* **2004**, *75*, 3242.
(50) Bazin, D.; Guczi, L. *Appl. Catal. A* **2001**, *213*, 147.
(51) Bergwerff, J. A.; van de Water, L. G. A.; Visser, T.; de Peinder, P.; Leliveld, B. R. G.; de Jong, K. P.; Weckhuysen, B. M. *Chem. Eur. J.* **2005**, *11*, 4592.
(52) van de Water, L. G. A.; Bergwerff, J. A.; Leliveld, B. R. G.; Weckhuysen, B. M.; de Jong, K. P. *J. Phys. Chem. B* **2005**, *109*, 14513.
(53) Michailowski, A.; Grunwaldt, J.-D.; Baiker, A.; Kiebach, R.; Bensch, W.; Patzke, G. R. *Angew. Chem.* **2005**, *44*, 5643.
(54) Clausen, B. S.; Topsøe, H. *Catal. Today* **1991**, *9*, 189.
(55) Guyot-Sionnest, N. S.; Villain, F.; Bazin, D.; Dexpert, H.; Lynch, J.; Lepeltier, F. *Catal. Lett.* **1991**, *8*, 283.
(56) Grunwaldt, J.-D.; Wandeler, R.; Baiker, A. *Catal. Rev. − Sci. Eng.* **2003**, *45*, 1.
(57) McBreen, J.; Mukerjee, S. *J. Electrochem. Soc.* **1995**, *142*, 3399.
(58) Russell, A. E.; Rose, A. *Chem. Rev.* **2004**, *104*, 4613.
(59) Roth, C.; Benker, N.; Buhrmester, T.; Mazurek, M.; Loster, M.; Fuess, H.; Koningsberger, D. C.; Ramaker, D. E. *J. Am. Chem. Soc.* **2005**, *127*, 14607.
(60) Vincze, L.; Vekemans, B.; Brenker, F. E.; Falkenberg, G.; Rickers, K.; Somogyi, A.; Kersten, M.; Adams, F. *Anal. Chem.* **2004**, *76*, 6786.
(61) Brown, G. E.; Sturchio, N. C. *Rev. Miner. Geochem.* **2002**, *49*, 1.
(62) Yun, W.; Pratt, S. T.; Miller, R. M.; Cai, Z.; Hunter, D. B.; Jarstfer, A. G.; Kemner, K. M.; Lai, B.; Lee, H. R.; Legnini, D. G.; Rodrigues, W.; Smith, C. I. *J. Synchrotron Radiat.* **1998**, *5*, 1390.
(63) Nakai, I.; Numako, C.; Hayakawa, S.; Tsuchiyama, A. *J. Trace Microprobe Tech.* **1998**, *16*, 87.
(64) Grolimund, D.; Senn, M.; Trottmann, M.; Janousch, M.; Bonhoure, I.; Marcus, M. *Spectrochim. Acta B* **2004**, *59*, 1627.
(65) Serrini, P.; Briois, V.; Horrillo, M. C.; Traverse, A.; Manes, L. *Thin Solid Films* **1997**, *304*, 113.
(66) Grandjean, D.; Benfield, R. E.; Nayral, C.; Maisonnat, A.; Chaudret, B. *J. Phys. Chem. B* **2004**, *108*, 8876.